

Proposal for realizing quantum-spin systems on a two-dimensional square lattice with Dzyaloshinskii-Moriya interaction by the Floquet engineering using Rydberg atoms

Hiroki Kuji,^{*} Masaya Kunimi,[†] and Tetsuro Nikuni[‡]

*Department of Physics, Tokyo University of Science,
1-3 Kagurazaka, Shinjuku, Tokyo 162-8601, Japan*

(Dated: November 12, 2024)

We theoretically propose a method for implementing the Hamiltonian incorporating Heisenberg and Dzyaloshinskii-Moriya (DM) interactions within Rydberg atoms arranged in a two-dimensional square lattice, utilizing Floquet engineering. In our scheme, we use both global and local operations of the spins. The global operations can be realized by applying the microwave and the local operations can be realized by the locally addressing lasers, which yields the ac-Stark shift. Since our engineered Hamiltonian contains bond-dependent DM interactions, we expect the emergence of quantum skyrmions in the ground state.

I. INTRODUCTION

Quantum simulation [1, 2], which involves the experimental emulation of specific physical systems, is a promising platform for addressing problems that are intractable with classical computers [3]. This approach has significantly contributed to the exploration of various quantum many-body phenomena using known platforms such as ultra-cold gases [4], trapped ions [5, 6], molecules [7, 8], and superconducting qubits [9–11]. Recently, a platform based on Rydberg atoms has attracted much attention due to its long coherence time, scalability, and high controllability via optical tweezers. Quantum simulations employing Rydberg atoms [12, 13] have been utilized to investigate various quantum many-body phenomena, such as quantum phases [14–17], nonequilibrium dynamics [18], and quantum thermalization [19, 20].

The Rydberg atom-based quantum simulator shows great potential for simulating quantum spin systems. However, it is limited to Hamiltonians that can be implemented. To date, one can experimentally realize quantum spin models as the Ising [16–18, 21–29], XY [15, 30, 31], XXZ [32–35] and XYZ [36, 37] models. There are several theoretical proposals for realizing a Hamiltonian with mono-axial Dzyaloshinskii-Moriya (DM) interactions [38–41] and Kitaev type interactions [38, 42, 43]. In this paper, we focus on the DM interaction [44, 45], which is defined by the outer product between two spins. This interaction is fundamental to various chiral magnetic structures, such as chiral solitons [46, 47] in one-dimensional systems and skyrmions [48–51] in higher dimensions. In particular, the full quantum calculation of the quantum skyrmions is a challenging task because the DM interaction causes the negative sign problem. Although the tensor network approach has been used for quantum skyrmions, it suffers from numerical errors in large system sizes [52]. Quan-

tum simulation using Rydberg atoms is an alternative approach for studying quantum skyrmions.

Floquet engineering is a powerful method for controlling Hamiltonian [53, 54]. Previous studies have experimentally demonstrated the realization of the XYZ Hamiltonian using global time-periodic operations [33, 36]. A theoretical proposal has also been made to implement a mono-axial DM interaction [38] using local operation [55, 56]. In this previous work, Nishad et al. proposed a method to engineer the Hamiltonian with the mono-axial DM interactions in a one-dimensional chain via the Floquet engineering [38]. However, the Hamiltonian with more complicated interaction, such as bond-dependent DM interaction, in higher dimensions has yet to be realized in the Rydberg atom quantum simulator.

In this paper, we propose a method to implement the Hamiltonian with Heisenberg and DM interactions in a Rydberg atom system arranged in a two-dimensional square lattice using the Floquet engineering approach. Our starting point is the XY Hamiltonian, which can be realized in the Rydberg atom systems [57–59]. By applying both time-periodic global and local pulses to the system, we can obtain the effective Hamiltonian that has the Heisenberg and bond-dependent DM interactions. We verify that our effective Hamiltonian can correctly reproduce the stroboscopic dynamics of the original Hamiltonian by numerical calculations. Our proposed experimental scheme is feasible with current state-of-the-art experimental techniques.

This paper is organized as follows: In Sec. II, we describe our model and theoretical methodology employed in this study. In Sec. III, we explain specific pulse sequences for implementing the Hamiltonian with the Heisenberg and DM interactions, and present numerical results that validate the proposed sequence. In Sec. IV, we summarize our results. In Appendices, we discuss the details of the calculations, the long-range interactions, and the symmetry properties of the effective Hamiltonian.

^{*} 1223518@ed.tus.ac.jp

[†] kunimi@rs.tus.ac.jp

[‡] nikuni@rs.tus.ac.jp

II. MODEL AND METHOD

In this study, we consider a system consisting of Rydberg atoms arranged in a two-dimensional square lattice with lattice spacing a . See Fig. 1(a). The position of the i th site is defined by $\mathbf{R}_i \equiv a(n_i \mathbf{e}_x + m_i \mathbf{e}_y)$, where n_i and m_i are integers, and $\mathbf{e}_{x,y}$ is the unit vector of each direction. We consider the spin-1/2 quantum spin systems. The two Rydberg states are mapped to the spin states $|nS\rangle = |\uparrow\rangle$ and $|nP\rangle = |\downarrow\rangle$ [15, 16, 30, 31, 36]. The states $|\uparrow_j\rangle$ and $|\downarrow_j\rangle$ denote the eigenstates of $\hat{S}_{\mathbf{R}_j}^z$ with eigenvalues $+1/2$ and $-1/2$, respectively, where $\hat{S}_{\mathbf{R}_j}^\alpha$ ($\alpha = x, y, z$) is the spin-1/2 operator at i th site. Because these two Rydberg states have opposite parity, the dipole-dipole interaction has nonzero matrix elements in the first-order perturbation for sufficiently large lattice spacing. In this setup, the Hamiltonian is given by the dipolar XY model [12, 15, 30, 31, 55, 60]:

$$\hat{H}_0 = \frac{1}{2} \sum_{i,j,i \neq j} J_{ij} (\hat{S}_{\mathbf{R}_i}^x \hat{S}_{\mathbf{R}_j}^x + \hat{S}_{\mathbf{R}_i}^y \hat{S}_{\mathbf{R}_j}^y), \quad (1)$$

where $J_{ij} \equiv 2C_3/|\mathbf{R}_i - \mathbf{R}_j|^3$ is the strength of the dipole-dipole interaction between i th and j th sites, and C_3 is the interaction constant. In this paper, we use open boundary conditions, and assume that the dipole-dipole interaction is isotropic, which can be realized by setting the quantization axis perpendicular to the xy -plane [12, 13].

We use the Floquet engineering [53, 54] to realize desired interaction Hamiltonian. In this scheme, we apply a time-periodic external field and focus on a timescale longer than the period of the external field. We consider the XY model Hamiltonian with an external field:

$$\hat{H}(t) = \hat{H}_0 + \hat{H}_{\text{drive}}(t), \quad (2)$$

where $\hat{H}_{\text{drive}}(t)$ represents the time-periodic external field. In the Floquet engineering, the time-evolution operator is defined as

$$\hat{U}(t) \equiv \mathcal{T} \exp \left[-\frac{i}{\hbar} \int_0^t dt' \hat{H}(t') \right], \quad (3)$$

$$\hat{H}(t) \equiv \hat{U}_{\text{drive}}^\dagger(t) \hat{H}_0 \hat{U}_{\text{drive}}(t), \quad (4)$$

$$\hat{U}_{\text{drive}}(t) \equiv \mathcal{T} \exp \left[-\frac{i}{\hbar} \int_0^t dt' \hat{H}_{\text{drive}}(t') \right], \quad (5)$$

where \mathcal{T} denotes the time-ordered product, and \hbar is the reduced Planck constant. The operator $\hat{H}(t)$ represents the Hamiltonian in the rotating frame. From the time evolution operator (3), we can define the Floquet Hamiltonian \hat{H}_F as

$$\hat{U}(T) = e^{-i\hat{H}_F T/\hbar}, \quad (6)$$

where T is the period of the external field.

The Floquet Hamiltonian reproduces the same time evolution at $t = nT$ as the Hamiltonian $\hat{H}(t)$, where n is an integer. In general, it is difficult to obtain the exact expression for the Floquet Hamiltonian. To do this, we use the Floquet-Magnus expansion [54, 61]. The leading term of the Floquet Hamiltonian is given by

$$\hat{H}_F^{(0)} = \frac{1}{T} \int_0^T dt \hat{H}(t). \quad (7)$$

Since this expansion is a short-time expansion, the timescale of the interaction is much longer than the period T , which implies $\max_{i,j} (|J_{ij}|)T/\hbar \ll 2\pi$.

By choosing the drive Hamiltonian $\hat{H}_{\text{drive}}(t)$ appropriately, we can obtain a desired effective Hamiltonian. To do this, we use two types of external fields: global operation, which uses microwave pulses to manipulate all atoms simultaneously, and local operation, which uses laser pulses to manipulate each atom individually [38]. See Figs. 1(b) and 1(c). To implement such pulses, we consider the following drive Hamiltonian:

$$\begin{aligned} \hat{H}_{\text{drive}}(t) &= \hat{H}_G(t) + \hat{H}_L(t) \\ &= \hbar\Omega(t) \sum_i [\cos \phi(t) \hat{S}_{\mathbf{R}_i}^x + \sin \phi(t) \hat{S}_{\mathbf{R}_i}^y] \\ &\quad + \hbar \sum_i \Delta_i(t) \hat{S}_{\mathbf{R}_i}^z, \end{aligned} \quad (8)$$

where $\hat{H}_G(t)$ is the global pulse term and $\hat{H}_L(t)$ is the local pulse term, which are defined by

$$\hat{H}_G(t) \equiv \hbar\Omega(t) \sum_i [\cos \phi(t) \hat{S}_{\mathbf{R}_i}^x + \sin \phi(t) \hat{S}_{\mathbf{R}_i}^y] \quad (9)$$

$$\hat{H}_L(t) \equiv \hbar \sum_i \Delta_i(t) \hat{S}_{\mathbf{R}_i}^z \quad (10)$$

$\Omega(t)$ is the time-dependent Rabi frequency of the drive, $\phi(t)$ is the phase, and $\Delta_i(t)$ is the space- and time-dependent ac-Stark shift. In this paper, we approximate the time dependence of the Rabi frequency $\Omega(t)$ and ac-Stark shift $\Delta(t)$ by delta functions, assuming that the pulses are applied to the system instantaneously. We denote the time interval between pulses by τ_i . We apply a two-step rotating-frame transformation with respect to the pulses for both global and local operations [38]. Under the above settings, we obtain the effective Hamiltonian:

$$\hat{H}_F^{(0)} = \frac{1}{T} \sum_i \hat{H}_i^{\text{rot}} \tau_i, \quad (11)$$

where \hat{H}_i^{rot} is the Hamiltonian in the rotating frame during the time interval τ_i . We choose the pulse sequence so that the effective Hamiltonian (11) becomes the desired Hamiltonian. Finally, the obtained pulse sequence in the rotating frame is transformed to derive the pulse sequence in the laboratory frame.

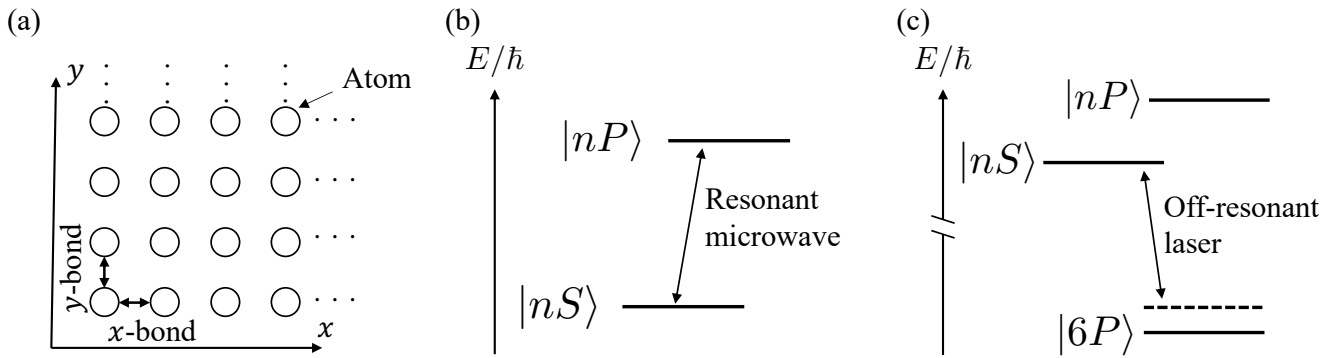


FIG. 1: (a) Schematic of the system in this study. (b) Schematic for global operations using microwave pulses. We can rotate all spins simultaneously by applying resonant microwave pulses, which couple $|nS\rangle$ and $|nP\rangle$ states. This operation corresponds to the uniform spin rotation around x - or y -axis. (c) Schematic for the local operation. By applying the off-resonant laser pulse to the individual atom, we can induce the site-dependent ac-Stark shift. This operation corresponds to the site-dependent spin rotation around z -axis.

In this work, we focus on the XYZ and DM interaction terms, which are defined by

$$\hat{H}_{XYZ} \equiv \frac{1}{2} \sum_{\mu=x,y,z} \sum_{i,j,i \neq j} J_{ij}^{\mu} \hat{S}_{\mathbf{R}_i}^{\mu} \hat{S}_{\mathbf{R}_j}^{\mu}, \quad (12)$$

$$\hat{H}_{DM} \equiv \frac{1}{2} \sum_{i,j,i \neq j} \mathbf{D}_{ij} \cdot (\hat{S}_{\mathbf{R}_i} \times \hat{S}_{\mathbf{R}_j}), \quad (13)$$

where J_{ij}^{μ} is the interaction strength of each spin component, and $\mathbf{D}_{ij} = -\mathbf{D}_{ji}$ is the DM vector. The XYZ Hamiltonian can be realized experimentally by applying the time-periodic global microwave pulses [33, 36]. The method to create a mono-axial DM interaction ($\mathbf{D}_{ij} \propto \mathbf{e}_z$) in the Rydberg atoms has been theoretically proposed [38]. This method is based on applying the local spin rotation around z axis (see Appendix A for details). Before presenting our results, we review the previous studies for the readers' convenience.

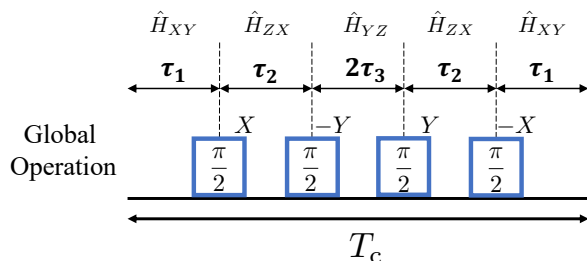


FIG. 2: Pulse sequence for creating the XYZ model Hamiltonians. Here, we present a sequence with one cycle period T_c . Global operation means applying the pulse to all trapped atoms. The angle $\pi/2$ denotes the rotation angle in the laboratory frame. The symbols $X, Y, -X$, and $-Y$ indicate the rotation axes. We list the Hamiltonian in the rotating frame in each time interval. The Floquet Hamiltonian can be obtained by averaging the listed terms.

First, we review Refs. [33, 36], which initially prepares the XY Hamiltonian (1), and implements the XYZ Hamiltonian by periodically applying pulses. The pulse operation for implementing the XYZ model Hamiltonian is shown in Fig. 2. It uses only four $\pi/2$ global rotations around the $\hat{S}^x, -\hat{S}^y, \hat{S}^y$, and $-\hat{S}^x$ axes. In $\hat{H}_G(t)$ of Eq. (11), this corresponds to setting the angle ϕ to $0, -\pi/2, \pi/2$, and π . The time intervals between pulses are given by τ_1, τ_2 , and $2\tau_3$. Then, by using the Floquet Magnus expansion, the effective Hamiltonian of the system can be written by

$$\hat{H}_F^{(0)} = \sum_{\langle i,j \rangle} \frac{2J_{ij}}{T_c} \left[(\tau_1 + \tau_2) \hat{S}_{\mathbf{R}_i}^x \hat{S}_{\mathbf{R}_j}^x + (\tau_1 + \tau_3) \hat{S}_{\mathbf{R}_i}^y \hat{S}_{\mathbf{R}_j}^y + (\tau_2 + \tau_3) \hat{S}_{\mathbf{R}_i}^z \hat{S}_{\mathbf{R}_j}^z \right], \quad (14)$$

where $T_c = 2(\tau_1 + \tau_2 + \tau_3)$ and $\sum_{\langle i,j \rangle}$ denotes the summation over the nearest-neighbor pairs.

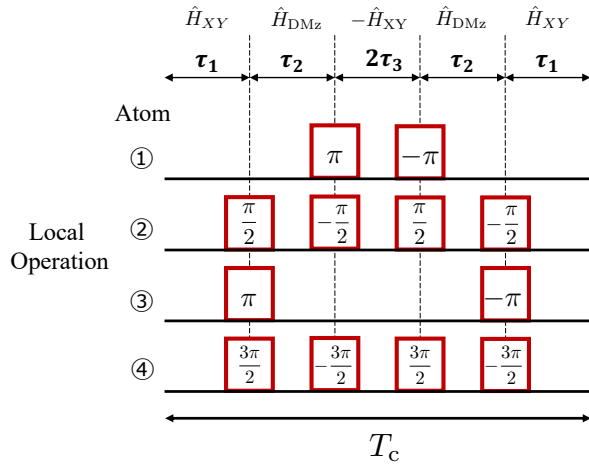


FIG. 3: Pulse sequence for creating the Hamiltonian with the mono-axial DM interaction. Here we show a sequence with one cycle period, denoted by T_c . Local operations refer to applying pulses to individual trapped atoms. The angles $\pm\pi/2, \pi, 3\pi/2$ indicate the rotation angles in the laboratory frame. All rotation axes are along \hat{S}^z -axis. We list the Hamiltonian of the rotating frame in each time interval. Here, we define $\hat{H}_{\text{DMz}} \equiv \sum_{\langle i,j \rangle} D_z (\hat{S}_{\mathbf{R}_i}^x \hat{S}_{\mathbf{R}_j}^y - \hat{S}_{\mathbf{R}_i}^y \hat{S}_{\mathbf{R}_j}^x)$.

Second, we review Ref. [38], which proposes a method for implementing the Hamiltonian with mono-axial DM interactions ($\mathbf{D}_{ij} \propto \mathbf{e}_z$) using local pulse operations. Figure 3 shows the proposed pulse sequence. Here, we consider the one-dimensional chain for simplicity. The pulse sequence consists of pulse operations so that the phase difference between neighboring atoms becomes $\pi/2$. By using the Floquet Magnus expansion, the effective Hamiltonian is obtained as

$$\hat{H}_{\text{F}}^{(0)} = \sum_{\langle i,j \rangle} \frac{2J_{ij}}{T_c} \left[(\tau_1 - \tau_3) (\hat{S}_{\mathbf{R}_i}^x \hat{S}_{\mathbf{R}_j}^x + \hat{S}_{\mathbf{R}_i}^y \hat{S}_{\mathbf{R}_j}^y) + \tau_2 (\hat{S}_{\mathbf{R}_i}^x \hat{S}_{\mathbf{R}_j}^y - \hat{S}_{\mathbf{R}_i}^y \hat{S}_{\mathbf{R}_j}^x) \right], \quad (15)$$

where \mathbf{R}_j represents the one-dimensional lattice position.

III. RESULTS

In two dimensions, various types of the DM interactions can exist. In this work, we propose a method to create the Bloch-type and Néel-type DM interactions [62, 63] in addition to the Heisenberg interactions. Before presenting our results, we explain our strategy for implementing these interactions using the Floquet engineering.

The DM vectors of the Bloch- and Néel-type DM interactions are given by $\mathbf{D}_{ij} \propto \mathbf{e}_x$ and $\propto \mathbf{e}_y$, respectively [see Eqs. (16) and (35)]. The key point for creating these terms is that the DM interactions can be obtained by applying a local spin rotation to the interaction terms

$\hat{h}_{ij}^{zx} \equiv \hat{S}_{\mathbf{R}_i}^z \hat{S}_{\mathbf{R}_j}^z + \hat{S}_{\mathbf{R}_i}^x \hat{S}_{\mathbf{R}_j}^x$ and $\hat{h}_{ij}^{yz} \equiv \hat{S}_{\mathbf{R}_i}^y \hat{S}_{\mathbf{R}_j}^y + \hat{S}_{\mathbf{R}_i}^z \hat{S}_{\mathbf{R}_j}^z$. For example, \hat{h}_{ij}^{zx} is transformed to $\hat{S}_{\mathbf{R}_i}^z \hat{S}_{\mathbf{R}_j}^z - \hat{S}_{\mathbf{R}_i}^x \hat{S}_{\mathbf{R}_j}^x$ after local spin rotation around \hat{S}^y -axis. For details on the relation between site-dependent spin rotation and the DM interaction, see Appendix A. Since the terms \hat{h}_{ij}^{zx} and \hat{h}_{ij}^{yz} appear after global $\pi/2$ spin rotation of the XY Hamiltonian around the \hat{S}^x - or \hat{S}^y -axis (see Fig. 2), we can obtain the Bloch- and Néel-type DM interactions combining the global and local pulse operations appropriately. The detailed methods for obtaining these two types of DM interactions are provided in Secs. III A and III B.

The resultant pulse sequence consists of 14 time intervals, from τ_1 to τ_{14} (see Figs. 4 and 5). We note that the validity of the Floquet Magnus expansion is determined by the total period of the pulse sequence T , which is given by the sum of all τ_j , rather than by each interval τ_j . For a typical interaction strength of the Rydberg atoms $J_0 \simeq h \times 250\text{kHz}$, the validity condition for the Floquet Magnus expansion $J_0 T / \hbar \ll 2\pi$ can be satisfied for $T \lesssim 1\mu\text{s}$, which is feasible with current experimental techniques [33, 36].

In the main text, we focus on the nearest-neighbor interactions between Rydberg atoms for simplicity [see Appendix B for a detailed derivation]. A discussion of long-range interaction, including next-nearest and next-next-nearest neighbors, is provided in Appendix C.

A. Bloch-type DM interaction

First, we consider the Bloch-type DM interaction. The target Hamiltonian is given by

$$\hat{H}_{\text{target}}^{\text{B}} = \sum_{\langle i,j \rangle} J_{ij}^{\text{ex}} (\hat{\mathbf{S}}_{\mathbf{R}_i} \cdot \hat{\mathbf{S}}_{\mathbf{R}_j}) + \sum_i \left[D_x (\hat{\mathbf{S}}_{\mathbf{R}_i} \times \hat{\mathbf{S}}_{\mathbf{R}_i + a\mathbf{e}_x})_x + D_y (\hat{\mathbf{S}}_{\mathbf{R}_i} \times \hat{\mathbf{S}}_{\mathbf{R}_i + a\mathbf{e}_y})_y \right], \quad (16)$$

where the J_{ij}^{ex} is the strength of the exchange interaction, and D_x and D_y represent the strength of the DM interaction along the x -bond and y -bond, respectively [see Fig. 1(a)]. The term $(\hat{\mathbf{S}}_{\mathbf{R}_i} \times \hat{\mathbf{S}}_{\mathbf{R}_j})_\alpha$ denotes the α -component of the outer product. This Hamiltonian can be realized by combining global and local operations within a single period. Our proposed pulse sequence is shown in Fig. 4. After applying the Floquet engineering, we obtain the following effective Hamiltonian [see

Hamiltonians in each time interval in the second rotating-frame

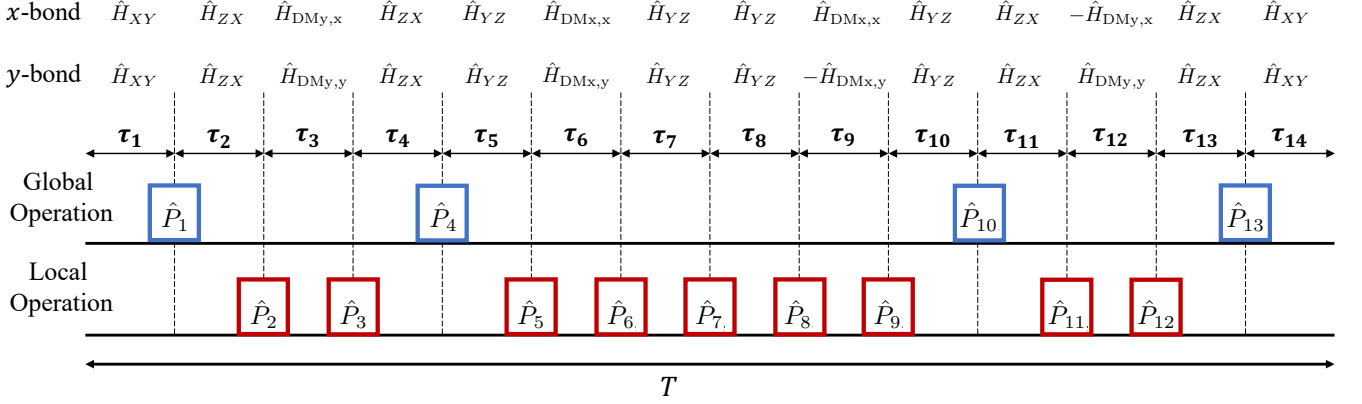


FIG. 4: Proposed pulse sequence for creating the Bloch-type DM interaction. Here, we show the sequence of a single period T . Global and local operations refer to applying the pulses to whole atoms and individual atoms, respectively. The operator \hat{P}_i denotes the pulse operator in the laboratory frame at time T_j . We list the Hamiltonian of the rotating frame in each time interval for each bond. Here, we define $\hat{H}_{DM_{\alpha,\beta}} \equiv \sum_i D_{\alpha}(\hat{\mathbf{S}}_{\mathbf{R}_i} \times \hat{\mathbf{S}}_{\mathbf{R}_i+ae_{\beta}})_{\alpha}$.

Appendix B for details]

$$\begin{aligned} \hat{H}_{\text{F}}^{(0)} &= \alpha_{XY} \hat{H}_{XY} + \alpha_{YZ} \hat{H}_{YZ} + \alpha_{ZX} \hat{H}_{ZX} \\ &+ \sum_i \frac{J}{T} \left[(\tau_6 + \tau_9) (\hat{\mathbf{S}}_{\mathbf{R}_i} \times \hat{\mathbf{S}}_{\mathbf{R}_i+ae_x})_x \right. \\ &+ (\tau_3 - \tau_{12}) (\hat{\mathbf{S}}_{\mathbf{R}_i} \times \hat{\mathbf{S}}_{\mathbf{R}_i+ae_y})_y \\ &+ (\tau_6 - \tau_9) (\hat{\mathbf{S}}_{\mathbf{R}_i} \times \hat{\mathbf{S}}_{\mathbf{R}_i+ae_y})_x \\ &\left. + (\tau_3 + \tau_{12}) (\hat{\mathbf{S}}_{\mathbf{R}_i} \times \hat{\mathbf{S}}_{\mathbf{R}_i+ae_y})_y \right], \end{aligned} \quad (17)$$

where $J \equiv 2C_3/a^3$ denotes the strength of the nearest-neighbor bare interaction, $\alpha_{XY} \equiv (\tau_1 + \tau_{14})/T$, $\alpha_{YZ} \equiv (\tau_5 + \tau_7 + \tau_8 + \tau_{10})/T$, $\alpha_{ZX} \equiv (\tau_2 + \tau_4 + \tau_{11} + \tau_{13})/T$, and we defined the following Hamiltonians:

$$\hat{H}_{XY} = J \sum_{\langle i,j \rangle} (\hat{S}_{\mathbf{R}_i}^x \hat{S}_{\mathbf{R}_j}^x + \hat{S}_{\mathbf{R}_i}^y \hat{S}_{\mathbf{R}_j}^y), \quad (18)$$

$$\hat{H}_{YZ} = J \sum_{\langle i,j \rangle} (\hat{S}_{\mathbf{R}_i}^y \hat{S}_{\mathbf{R}_j}^y + \hat{S}_{\mathbf{R}_i}^z \hat{S}_{\mathbf{R}_j}^z), \quad (19)$$

$$\hat{H}_{ZX} = J \sum_{\langle i,j \rangle} (\hat{S}_{\mathbf{R}_i}^z \hat{S}_{\mathbf{R}_j}^z + \hat{S}_{\mathbf{R}_i}^x \hat{S}_{\mathbf{R}_j}^x). \quad (20)$$

To implement the target Hamiltonian (16), we set the propagation times as $\tau_1 + \tau_{14} = \tau_2 + \tau_4 + \tau_{11} + \tau_{13} = \tau_5 + \tau_7 + \tau_8 + \tau_{10} \equiv \tau$, $\tau_6 = \tau_9 \equiv \tau_x$, and $\tau_3 = \tau_{12} \equiv \tau_y$. The effective Hamiltonian then becomes

$$\begin{aligned} \hat{H}_{\text{F,Bloch}}^{(0)} &= J_{\text{F}} \sum_{\langle i,j \rangle} \hat{\mathbf{S}}_{\mathbf{R}_i} \cdot \hat{\mathbf{S}}_{\mathbf{R}_j} \\ &+ \sum_i \left[D_{x,\text{F}} (\hat{\mathbf{S}}_{\mathbf{R}_i} \times \hat{\mathbf{S}}_{\mathbf{R}_i+ae_x})_x \right. \\ &\quad \left. + D_{y,\text{F}} (\hat{\mathbf{S}}_{\mathbf{R}_i} \times \hat{\mathbf{S}}_{\mathbf{R}_i+ae_y})_y \right], \end{aligned} \quad (21)$$

where we have defined $J_{\text{F}} = J\tau/T$, $D_{x,\text{F}} = J\tau_x/T$, and $D_{y,\text{F}} = J\tau_y/T$. We note that the period T can be written as $T = \sum_{k=1}^{14} \tau_k$. Although the ratio between the exchange interaction and DM interaction J/D can be tuned from 0 to ∞ by changing the time interval, there are practical limitations of tuning the ratio J/D due to the experimental constraints, such as the finite pulse width.

Here, we show the pulse sequence for creating the Bloch-type DM interaction. Let \hat{P}_i be a unitary operator representing the time evolution at time $T_i \equiv \sum_{k=1}^i \tau_k$. This operator describes the time evolution in the laboratory frame. The expressions are given by [see Appendix B

for details]

$$\hat{P}_1 = \exp\left(-i\hat{S}_{\text{tot}}^x\pi/2\right), \quad (22)$$

$$\hat{P}_2 = \exp\left\{-i\sum_j[\hat{S}_{\mathbf{R}_j}^z(2\pi - (n_j + m_j)\pi/2)]\right\}, \quad (23)$$

$$\hat{P}_3 = \hat{P}_2^\dagger, \quad (24)$$

$$\hat{P}_4 = \exp\left(+i\hat{S}_{\text{tot}}^y\pi/2\right), \quad (25)$$

$$\hat{P}_5 = \hat{P}_2, \quad (26)$$

$$\hat{P}_6 = \hat{P}_3, \quad (27)$$

$$\hat{P}_7 = \hat{1}, \quad (28)$$

$$\hat{P}_8 = \exp\left\{-i\sum_j[\hat{S}_{\mathbf{R}_j}^z(2\pi + (m_j - n_j)\pi/2)]\right\}, \quad (29)$$

$$\hat{P}_9 = \hat{P}_8^\dagger, \quad (30)$$

$$\hat{P}_{10} = \hat{P}_4^\dagger, \quad (31)$$

$$\hat{P}_{11} = \exp\left\{-i\sum_j[\hat{S}_{\mathbf{R}_j}^z(2\pi + (n_j - m_j)\pi/2)]\right\}, \quad (32)$$

$$\hat{P}_{12} = \hat{P}_{11}^\dagger, \quad (33)$$

$$\hat{P}_{13} = \hat{P}_1^\dagger, \quad (34)$$

where $\hat{S}_{\text{tot}}^\alpha = \sum_j \hat{S}_{\mathbf{R}_j}^\alpha$ and $\hat{1}$ represents the identity operator.

B. Néel-type DM interaction

Here, we discuss how to create the Néel-type DM interaction. The target Hamiltonian is given by

$$\begin{aligned} \hat{H}_{\text{target}}^N = & \sum_{\langle i,j \rangle} J_{ij}(\hat{\mathbf{S}}_{\mathbf{R}_i} \cdot \hat{\mathbf{S}}_{\mathbf{R}_j}) \\ & + \sum_i \left[D_y(\hat{\mathbf{S}}_{\mathbf{R}_i} \times \hat{\mathbf{S}}_{\mathbf{R}_i + a\mathbf{e}_x})_y \right. \\ & \left. + D_x(\hat{\mathbf{S}}_{\mathbf{R}_i} \times \hat{\mathbf{S}}_{\mathbf{R}_i + a\mathbf{e}_y})_x \right]. \end{aligned} \quad (35)$$

This Hamiltonian can be realized by slightly modifying the pulse sequence used for the Bloch-type DM interaction. We replace \hat{P}_8 and \hat{P}_{11} with

$$\hat{P}_8 = \exp\left\{\sum_j[-i\hat{S}_{\mathbf{R}_j}^z(2\pi - (m_j - n_j)\pi/2)]\right\}, \quad (36)$$

$$\hat{P}_{11} = \exp\left\{\sum_j[-i\hat{S}_{\mathbf{R}_j}^z(2\pi - (n_j - m_j)\pi/2)]\right\}. \quad (37)$$

Using the pulse sequence shown in Fig. 5, we obtain the effective Hamiltonian

$$\begin{aligned} \hat{H}_{\text{F}}^{(0)} = & \alpha_{XY}\hat{H}_{XY} + \alpha_{YZ}\hat{H}_{YZ} + \alpha_{ZX}\hat{H}_{ZX} \\ & + \sum_i \frac{J}{T} \left[(\tau_6 - \tau_9)(\hat{\mathbf{S}}_{\mathbf{R}_i} \times \hat{\mathbf{S}}_{\mathbf{R}_i + a\mathbf{e}_x})_x \right. \\ & + (\tau_3 + \tau_{12})(\hat{\mathbf{S}}_{\mathbf{R}_i} \times \hat{\mathbf{S}}_{\mathbf{R}_i + a\mathbf{e}_x})_y \\ & + (\tau_6 + \tau_9)(\hat{\mathbf{S}}_{\mathbf{R}_i} \times \hat{\mathbf{S}}_{\mathbf{R}_i + a\mathbf{e}_y})_x \\ & \left. + (\tau_3 - \tau_{12})(\hat{\mathbf{S}}_{\mathbf{R}_i} \times \hat{\mathbf{S}}_{\mathbf{R}_i + a\mathbf{e}_y})_y \right]. \end{aligned} \quad (38)$$

Setting the pulse interval appropriately, we obtain the target Hamiltonian (Eq. 35).

C. Numerical Analysis

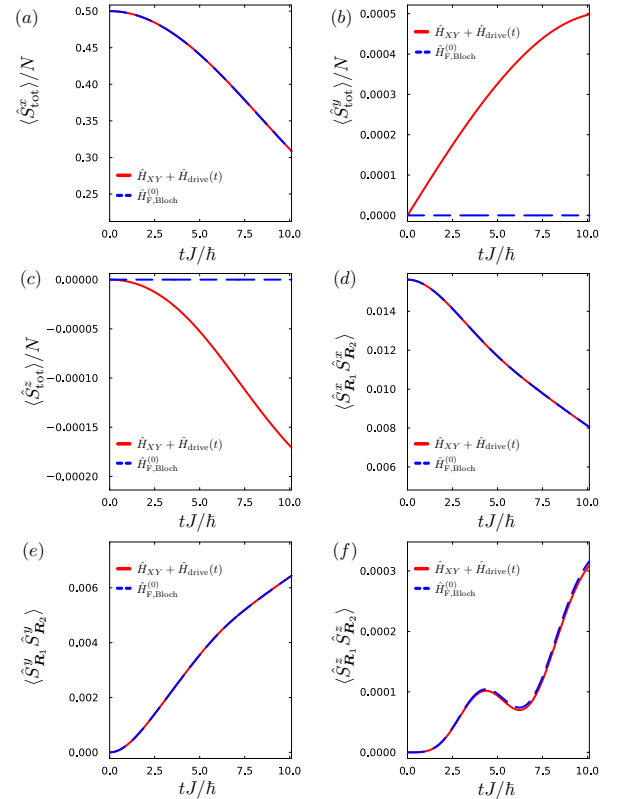


FIG. 6: Time evolution of the spin expectation value $\langle \hat{S}_{\text{tot}}^\alpha \rangle / N$ for (a) $\alpha = x$, (b) $\alpha = y$, and (c) $\alpha = z$. The time evolution of the two-body correlation function $\langle \hat{S}_{\mathbf{R}_i}^\alpha \hat{S}_{\mathbf{R}_i}^\alpha \rangle$ for (d) $\alpha = x$, (e) $\alpha = y$, and (f) $\alpha = z$. The solid red (dashed blue) line represents the results of the time-evolution under the original Hamiltonian $\hat{H}_{XY} + \hat{H}_{\text{drive}}(t)$ (the Bloch-type effective Hamiltonian $\hat{H}_{\text{F,Bloch}}^{(0)}$)

We show the numerical results of the spin expectation value in Figs. 6(a), (b), and (c). The time evolution of \hat{S}_{tot}^x under the effective Hamiltonian is in good

Hamiltonians in each time interval in the second rotating-frame

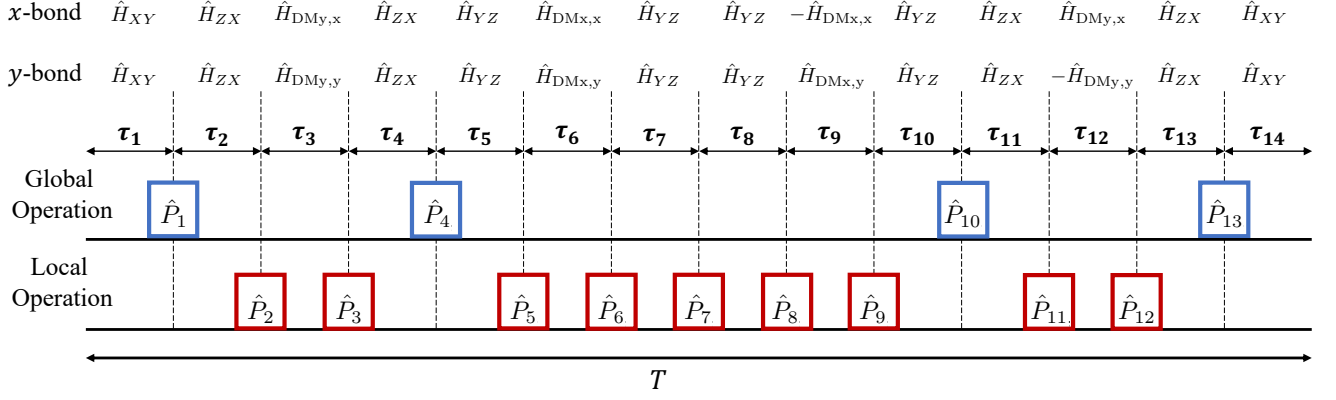


FIG. 5: Proposed pulse sequence for creating the Néel type DM interaction. Here, we show the sequence of a single period T . Global and local operations refer to applying the pulses to whole atoms and individual atoms, respectively. The operator \hat{P}_i denotes the pulse operator in the laboratory frame at time T_j . We list the Hamiltonian of the rotating frame in each time interval for each bond.

agreement with that under the original Hamiltonian as shown in Fig. 6(a). However, we find that the clear deviation for \hat{S}_{tot}^y and \hat{S}_{tot}^z as shown in Figs. 6(b) and (c). Under the time evolution associated with the effective Hamiltonian, the expectation values of \hat{S}_{tot}^y and \hat{S}_{tot}^z are always zero at any time. These results are due to a symmetry of the effective Hamiltonian [see Appendix D for details]. The exact Hamiltonian has no such symmetry possessed by the effective Hamiltonian. Therefore, the expectation values of \hat{S}_{tot}^y and \hat{S}_{tot}^z deviate from zero in the exact time evolution. If we consider the higher-order term of the Magnus expansion, the Floquet Hamiltonian might describe this deviation. In Figs. 6(d), (e), and (f), we show the time evolution of the correlation functions $\langle \hat{S}_{\mathbf{R}_1}^\alpha \hat{S}_{\mathbf{R}_2}^\alpha \rangle$ ($\alpha = x, y, z$), where $\mathbf{R}_1 = (0, 0)$ and $\mathbf{R}_2 = (a, 0)$. We can see good agreement with the exact and effective Hamiltonian. From these results, we conclude that our proposed pulse scheme can successfully implement the effective Hamiltonian.

Finally, we discuss the validity of the lowest-order Magnus expansion in our systems. As discussed in Sec. II and previous paragraph of this section, the Magnus expansion is a high frequency expansion. The accuracy of the method depends on the period T of the time-periodic external field. To see explicitly how the period T affects the validity of the expansion, we calculate the time evolution of the correlation function $\langle \hat{S}_{\mathbf{R}_1}^x \hat{S}_{\mathbf{R}_2}^x \rangle$ for the same interaction parameters as Fig. 6, but for different periods T . The results are shown in Figs. 7(a), 7(b), and 7(c). In the short-period regime ($JT/\hbar \lesssim 2\pi$), the lowest-order Magnus expansion agrees well with the exact results as shown in Figs. 7(a) and 7(b). On the other hand, in the case of long period ($JT/\hbar \sim 2\pi$) case, we can see a clear deviation between the lowest-order Magnus expansion and exact results for $T = 2.8\hbar/J$, as shown in Fig. 7(c). This

discrepancy indicates that, for shorter periods, it is necessary to incorporate higher-order contributions in the Magnus expansion.

IV. SUMMARY

In conclusion, we have proposed a method to create the effective Hamiltonian incorporating the Heisenberg interactions and two-dimensional DM interactions through the Floquet engineering. This approach utilizes both local and global operations tailored for Rydberg atoms arranged in a two-dimensional square lattice. The strength of each interaction in the proposed Hamiltonian is controllable by tuning the pulse intervals. Numerical simulations have validated the effectiveness of our proposed sequence.

All pulse operations in our method can be feasibly implemented using state-of-the-art experimental techniques. Indeed, global operation [33, 36] and local operation [38, 56] are each implemented by the experiment.

However, it is worth noting that when employing local operation, the number of lasers required scales proportionally with the number of atoms. This consideration is typically manageable within the context of optical tweezers research.

In this study, we implemented a Hamiltonian with Heisenberg and DM interactions on a two-dimensional square lattice. This research represents a step towards the future implementation of quantum simulations of the Hamiltonian for arbitrary quantum spin systems. We consider that the implemented Hamiltonian can be utilized to explore novel quantum many-body phenomena and contribute to the investigation of the microscopic behavior of quantum skyrmion by implementing a regime where quantum fluctuations are significant.

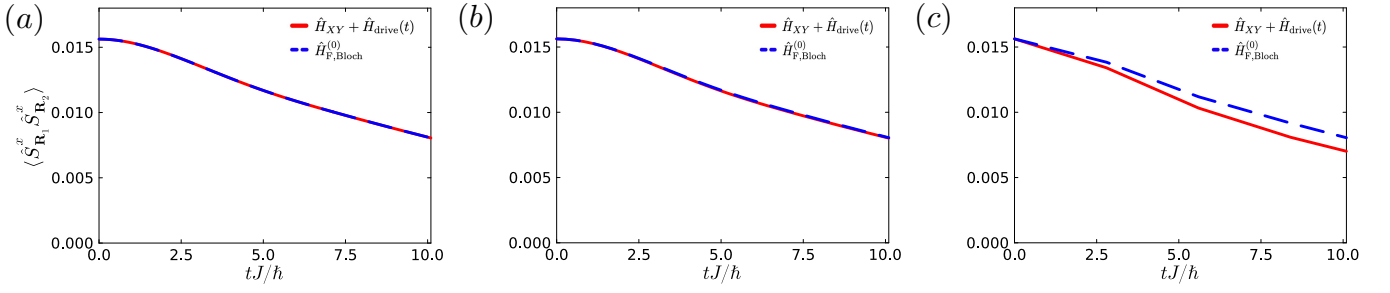


FIG. 7: Time evolution of the two-body correlation function $\langle \hat{S}_{\mathbf{R}_1}^x \hat{S}_{\mathbf{R}_2}^x \rangle$ for different periods T : (a) $T = 0.028\hbar/J$, (b) $T = 0.28\hbar/J$, and (c) $T = 2.8\hbar/J$.

The solid red line shows the time-evolution under the original Hamiltonian $\hat{H}_{XY} + \hat{H}_{\text{drive}}(t)$, while the dashed blue line represents the results under the Bloch-type effective Hamiltonian $\hat{H}_{\text{F,Bloch}}^{(0)}$.

ACKNOWLEDGMENTS

We thank T. Tomita for his useful comments. This work was supported by JSPS KAKENHI Grants No. JP22H05268 (M.K.).

Appendix A: Relation between site-dependent spin rotation and DM interaction

This Appendix discusses the relation between the site-dependent spin rotation and DM interaction. We consider the following Hamiltonians:

$$\hat{H}_{XY} = J \sum_{\langle j,k \rangle} (\hat{S}_{\mathbf{R}_j}^x \hat{S}_{\mathbf{R}_k}^x + \hat{S}_{\mathbf{R}_j}^y \hat{S}_{\mathbf{R}_k}^y), \quad (\text{A1})$$

$$\hat{H}_{YZ} = J \sum_{\langle j,k \rangle} (\hat{S}_{\mathbf{R}_j}^y \hat{S}_{\mathbf{R}_k}^y + \hat{S}_{\mathbf{R}_j}^z \hat{S}_{\mathbf{R}_k}^z), \quad (\text{A2})$$

$$\hat{H}_{ZX} = J \sum_{\langle j,k \rangle} (\hat{S}_{\mathbf{R}_j}^z \hat{S}_{\mathbf{R}_k}^z + \hat{S}_{\mathbf{R}_j}^x \hat{S}_{\mathbf{R}_k}^x), \quad (\text{A3})$$

where we consider only nearest-neighbor interaction. We employ the following spin rotation operator [38, 39]:

$$\hat{U}_{\text{rot},\alpha} \equiv \exp \left(-i \sum_j \hat{S}_{\mathbf{R}_j}^\alpha \phi_j \right), \quad (\text{A4})$$

where ϕ_j represents the rotation angle at the j th site. By direct calculations, we can obtain the following relations:

$$\hat{U}_{\text{rot},z}^\dagger \hat{H}_{XY} \hat{U}_{\text{rot},z} = J \sum_{\langle j,k \rangle} \left[\cos(\phi_j - \phi_k) (\hat{S}_{\mathbf{R}_j}^x \hat{S}_{\mathbf{R}_k}^x + \hat{S}_{\mathbf{R}_j}^y \hat{S}_{\mathbf{R}_k}^y) + \sin(\phi_j - \phi_k) (\hat{S}_{\mathbf{R}_j}^x \hat{S}_{\mathbf{R}_k}^y - \hat{S}_{\mathbf{R}_j}^y \hat{S}_{\mathbf{R}_k}^x) \right], \quad (\text{A5})$$

$$\hat{U}_{\text{rot},x}^\dagger \hat{H}_{YZ} \hat{U}_{\text{rot},x} = J \sum_{\langle j,k \rangle} \left[\cos(\phi_j - \phi_k) (\hat{S}_{\mathbf{R}_j}^y \hat{S}_{\mathbf{R}_k}^y + \hat{S}_{\mathbf{R}_j}^z \hat{S}_{\mathbf{R}_k}^z) + \sin(\phi_j - \phi_k) (\hat{S}_{\mathbf{R}_j}^y \hat{S}_{\mathbf{R}_k}^z - \hat{S}_{\mathbf{R}_j}^z \hat{S}_{\mathbf{R}_k}^y) \right], \quad (\text{A6})$$

$$\hat{U}_{\text{rot},y}^\dagger \hat{H}_{ZX} \hat{U}_{\text{rot},y} = J \sum_{\langle j,k \rangle} \left[\cos(\phi_j - \phi_k) (\hat{S}_{\mathbf{R}_j}^z \hat{S}_{\mathbf{R}_k}^z + \hat{S}_{\mathbf{R}_j}^x \hat{S}_{\mathbf{R}_k}^x) + \sin(\phi_j - \phi_k) (\hat{S}_{\mathbf{R}_j}^z \hat{S}_{\mathbf{R}_k}^x - \hat{S}_{\mathbf{R}_j}^x \hat{S}_{\mathbf{R}_k}^z) \right]. \quad (\text{A7})$$

From the above results, by taking $\phi_j - \phi_k = \pi/2$, the DM interaction for each component of the DM vector is obtained.

Appendix B: Derivation of the nearest-neighbor part of the effective Hamiltonian

This Appendix discusses the engineering of the Hamiltonian with the Heisenberg and Bloch-type DM interaction in detail. The Hamiltonian with Néel-type DM interaction can be obtained by a similar calculation. The target Hamiltonian is

$$\hat{H}_{\text{target}}^{\text{B}} = J \sum_{\langle i,j \rangle} \hat{\mathbf{S}}_{\mathbf{R}_i} \cdot \hat{\mathbf{S}}_{\mathbf{R}_j} + \sum_i \left[D_x (\hat{\mathbf{S}}_{\mathbf{R}_i} \times \hat{\mathbf{S}}_{\mathbf{R}_i + a\mathbf{e}_x})_x + D_y (\hat{\mathbf{S}}_{\mathbf{R}_i} \times \hat{\mathbf{S}}_{\mathbf{R}_i + a\mathbf{e}_y})_y \right]. \quad (\text{B1})$$

The Hamiltonian in the laboratory frame is given by

$$\hat{H}(t) = \hat{H}_{XY} + \hat{H}_{\text{drive}}(t), \quad (\text{B2})$$

$$\begin{aligned} \hat{H}_{\text{drive}}(t) &= \hat{H}_{\text{G}}(t) + \hat{H}_{\text{L}}(t) \\ &= \hbar\Omega(t) \sum_i [\cos \phi(t) \hat{S}_{\mathbf{R}_i}^x + \sin \phi(t) \hat{S}_{\mathbf{R}_i}^y] + \hbar \sum_i \Delta_i(t) \hat{S}_{\mathbf{R}_i}^z, \end{aligned} \quad (\text{B3})$$

where $\hat{H}_{\text{G}}(t)$ is the global pulse term and $\hat{H}_{\text{L}}(t)$ is the local pulse term. Here, the global pulse is chosen as in the case of the XYZ Hamiltonian [33, 36], and thus the sequence becomes $(\hat{S}^x, -\hat{S}^y, \hat{S}^y, -\hat{S}^x)$ of four $\pi/2$ microwave pulses. The time evolution operator can be written as

$$\begin{aligned} \hat{U}_{\text{G}}(t) &\equiv \mathcal{T} \exp \left[-\frac{i}{\hbar} \int_0^t dt' \hat{H}_{\text{G}}(t') \right] \\ &= \begin{cases} \hat{1} & 0 \leq t < T_1, \\ e^{-i\hat{S}_{\text{tot}}^x \pi/2} & T_1 \leq t < T_4, \\ e^{i\hat{S}_{\text{tot}}^y \pi/2} e^{-i\hat{S}_{\text{tot}}^x \pi/2} & T_4 \leq t < T_{10}, \\ e^{i\hat{S}_{\text{tot}}^x \pi/2} & T_{10} \leq t < T_{13}, \\ \hat{1} & T_{13} \leq t < T. \end{cases} \end{aligned} \quad (\text{B4})$$

The Hamiltonian in the first rotating frame is given by

$$\hat{H}_1(t) \equiv \hat{U}_G^\dagger(t)[\hat{H}_{XY} + \hat{H}_L(t)]\hat{U}_G(t) \equiv \hat{H}_{XY1}(t) + \hat{H}_{L1}(t), \quad (\text{B5})$$

where

$$\hat{H}_{XY1}(t) = \begin{cases} \hat{H}_{XY} & 0 \leq t < T_1, \\ \hat{H}_{ZX} & T_1 \leq t < T_4, \\ \hat{H}_{YZ} & T_4 \leq t < T_{10}, \\ \hat{H}_{ZX} & T_{10} \leq t < T_{13}, \\ \hat{H}_{XY} & T_{13} \leq t < T, \end{cases} \quad (\text{B6})$$

$$\hat{H}_{L1}(t) = \hat{U}_G^\dagger(t)\hat{H}_L(t)\hat{U}_G(t). \quad (\text{B7})$$

Next, we consider the second rotating frame. In this frame, the Hamiltonian is given by

$$\hat{H}_2(t) = \hat{U}_L^\dagger(t)\hat{H}_{XY1}(t)\hat{U}_L(t), \quad (\text{B8})$$

$$\hat{U}_L(t) \equiv \mathcal{T} \exp \left[-\frac{i}{\hbar} \int_0^t dt' \hat{H}_{L1}(t') \right]. \quad (\text{B9})$$

Because our pulse sequence is a piecewise function of time, we can write $\hat{U}_L(t)$ as

$$\hat{U}_L(t) = \hat{V}_k, \quad \text{for } T_k \leq t < T_{k+1}, \quad (\text{B10})$$

$$\hat{V}_k \equiv \hat{V}_k \hat{V}_{k-1} \cdots \hat{V}_1 \hat{V}_0, \quad (\text{B11})$$

where \hat{V}_k is the time evolution operator at time T_k in the first rotating frame. The effective Hamiltonian is given by

$$\begin{aligned} \hat{H}_F^{(0)} &\equiv \frac{1}{T} \int_0^T dt \hat{H}_2(t) \\ &= \frac{1}{T} \sum_{k=1}^{14} \hat{V}_{k-1}^\dagger \hat{H}_k \hat{V}_{k-1} \tau_k, \end{aligned} \quad (\text{B12})$$

where \hat{H}_k represents $\hat{H}_{XY1}(t)$ during the time interval τ_k . From these results, we choose \hat{V}_j to create the target Hamiltonian. The results are given by

$$\hat{U}_L(t) = \begin{cases} \hat{V}_0 = \hat{1}, & 0 \leq t < T_1, \\ \hat{V}_1 = \hat{1}, & T_1 \leq t < T_2, \\ \hat{V}_2 = \exp \left\{ -i \sum_j [\hat{S}_{\mathbf{R}_j}^y (2\pi - (n_j + m_j)\pi/2)] \right\}, & T_2 \leq t < T_3, \\ \hat{V}_3 = \hat{1}, & T_3 \leq t < T_4, \\ \hat{V}_4 = \hat{1}, & T_4 \leq t < T_5, \\ \hat{V}_5 = \exp \left\{ -i \sum_j [\hat{S}_{\mathbf{R}_j}^x (2\pi - (n_j + m_j)\pi/2)] \right\}, & T_5 \leq t < T_6, \\ \hat{V}_6 = \hat{1}, & T_6 \leq t < T_7, \\ \hat{V}_7 = \hat{1}, & T_7 \leq t < T_8, \\ \hat{V}_8 = \exp \left\{ -i \sum_j [\hat{S}_{\mathbf{R}_j}^x (2\pi + (m_j - n_j)\pi/2)] \right\}, & T_8 \leq t < T_9, \\ \hat{V}_9 = \hat{1}, & T_9 \leq t < T_{10}, \\ \hat{V}_{10} = \hat{1}, & T_{10} \leq t < T_{11}, \\ \hat{V}_{11} = \exp \left\{ -i \sum_j [\hat{S}_{\mathbf{R}_j}^y (2\pi + (n_j - m_j)\pi/2)] \right\}, & T_{11} \leq t < T_{12}, \\ \hat{V}_{12} = \hat{1}, & T_{12} \leq t < T_{13}, \\ \hat{V}_{13} = \hat{1}, & T_{13} \leq t < T. \end{cases} \quad (\text{B13})$$

Using Eq. (B11), we obtain the expressions for \hat{V}_j :

$$\hat{V}_0 = \hat{1}, \quad (\text{B14})$$

$$\hat{V}_1 = \hat{1}, \quad (\text{B15})$$

$$\hat{V}_2 = \exp \left\{ -i \sum_j [\hat{S}_{\mathbf{R}_j}^y (2\pi - (n_j + m_j)\pi/2)] \right\}, \quad (\text{B16})$$

$$\hat{V}_3 = \exp \left\{ +i \sum_j [\hat{S}_{\mathbf{R}_j}^y (2\pi - (n_j + m_j)\pi/2)] \right\}, \quad (\text{B17})$$

$$\hat{V}_4 = \hat{1}, \quad (\text{B18})$$

$$\hat{V}_5 = \exp \left\{ -i \sum_j [\hat{S}_{\mathbf{R}_j}^x (2\pi - (n_j + m_j)\pi/2)] \right\}, \quad (\text{B19})$$

$$\hat{V}_6 = \exp \left\{ +i \sum_j [\hat{S}_{\mathbf{R}_j}^x (2\pi - (n_j + m_j)\pi/2)] \right\}, \quad (\text{B20})$$

$$\hat{V}_7 = \hat{1}, \quad (\text{B21})$$

$$\hat{V}_8 = \exp \left\{ -i \sum_j [\hat{S}_{\mathbf{R}_j}^x (2\pi + (m_j - n_j)\pi/2)] \right\}, \quad (\text{B22})$$

$$\hat{V}_9 = \exp \left\{ +i \sum_j [\hat{S}_{\mathbf{R}_j}^x (2\pi + (m_j - n_j)\pi/2)] \right\}, \quad (\text{B23})$$

$$\hat{V}_{10} = \hat{1}, \quad (\text{B24})$$

$$\hat{V}_{11} = \exp \left\{ -i \sum_j [\hat{S}_{\mathbf{R}_j}^y (2\pi + (n_j - m_j)\pi/2)] \right\}, \quad (\text{B25})$$

$$\hat{V}_{12} = \exp \left\{ +i \sum_j [\hat{S}_{\mathbf{R}_j}^y (2\pi + (n_j - m_j)\pi/2)] \right\}, \quad (\text{B26})$$

$$\hat{V}_{13} = \hat{1}. \quad (\text{B27})$$

The effective Hamiltonian becomes

$$\begin{aligned} \hat{H}_{\text{F}}^{(0)} &= \frac{1}{T} \sum_{k=1}^{14} \hat{V}_{k-1}^\dagger \hat{H}_k \hat{V}_{k-1} \tau_k \\ &= \alpha_{XY} \hat{H}_{XY} + \alpha_{YZ} \hat{H}_{YZ} + \alpha_{XZ} \hat{H}_{ZX} + \sum_i \frac{J}{T} \left[(\tau_6 + \tau_9) (\hat{\mathbf{S}}_{\mathbf{R}_i} \times \hat{\mathbf{S}}_{\mathbf{R}_i + a\mathbf{e}_x})_x \right. \\ &\quad \left. + (\tau_3 - \tau_{12}) (\hat{\mathbf{S}}_{\mathbf{R}_i} \times \hat{\mathbf{S}}_{\mathbf{R}_i + a\mathbf{e}_x})_y + (\tau_6 - \tau_9) (\hat{\mathbf{S}}_{\mathbf{R}_i} \times \hat{\mathbf{S}}_{\mathbf{R}_i + a\mathbf{e}_y})_x + (\tau_3 + \tau_{12}) (\hat{\mathbf{S}}_{\mathbf{R}_i} \times \hat{\mathbf{S}}_{\mathbf{R}_i + a\mathbf{e}_y})_y \right]. \end{aligned} \quad (\text{B28})$$

To implement the target Hamiltonian, we set the propagation times as $\tau_1 + \tau_{14} = \tau_2 + \tau_4 + \tau_{11} + \tau_{13} = \tau_5 + \tau_7 + \tau_8 + \tau_{10} = \tau$, $\tau_6 = \tau_9 = \tau_x$, and $\tau_3 = \tau_{12} = \tau_y$. The effective Hamiltonian then reduces to the target Hamiltonian:

$$\hat{H}_{\text{F}}^{(0)} = J_{\text{F}} \sum_{\langle i,j \rangle} \hat{\mathbf{S}}_{\mathbf{R}_i} \cdot \hat{\mathbf{S}}_{\mathbf{R}_j} + \sum_i \left[D_{x,\text{F}} (\hat{\mathbf{S}}_{\mathbf{R}_i} \times \hat{\mathbf{S}}_{\mathbf{R}_i + a\mathbf{e}_x})_x + D_{y,\text{F}} (\hat{\mathbf{S}}_{\mathbf{R}_i} \times \hat{\mathbf{S}}_{\mathbf{R}_i + a\mathbf{e}_y})_y \right]. \quad (\text{B29})$$

Finally, we consider the transformation of the time evolution operator in the rotating frame to the laboratory frame, which is required for the experiments. We consider the time evolution operator given by

$$\begin{aligned} \hat{U}(t) &= \mathcal{T} \exp \left[-\frac{i}{\hbar} \int_0^t dt' \hat{H}_{\text{drive}}(t') \right] \\ &= \hat{\mathcal{P}}_k, \quad \text{for } T_k \leq t < T_{k+1}, \end{aligned} \quad (\text{B30})$$

$$\hat{\mathcal{P}}_k \equiv \hat{P}_k \hat{P}_{k-1} \cdots \hat{P}_1 \hat{P}_0, \quad (\text{B31})$$

where we used the fact that the pulse sequence is a piecewise function of time. Using $\hat{H}_{\text{drive}}(t) = \hat{H}_{\text{G}}(t) +$

$\hat{U}_G(t)\hat{H}_{L1}(t)\hat{U}_G^\dagger(t)$, we obtain the time evolution operator in the laboratory frame:

$$\hat{U}(t) = \begin{cases} \hat{\mathcal{P}}_0 = \hat{1} & 0 \leq t < T_1, \\ \hat{\mathcal{P}}_1 = \hat{P}_1 & T_1 \leq t < T_2, \\ \hat{\mathcal{P}}_2 = \hat{P}_2\hat{P}_1 & T_2 \leq t < T_3, \\ \hat{\mathcal{P}}_3 = \hat{P}_1 & T_3 \leq t < T_4, \\ \hat{\mathcal{P}}_4 = \hat{P}_4\hat{P}_1 & T_4 \leq t < T_5, \\ \hat{\mathcal{P}}_5 = \hat{P}_5\hat{P}_4\hat{P}_1 & T_5 \leq t < T_6, \\ \hat{\mathcal{P}}_6 = \hat{P}_4\hat{P}_1 & T_6 \leq t < T_7, \\ \hat{\mathcal{P}}_7 = \hat{P}_4\hat{P}_1 & T_7 \leq t < T_8, \\ \hat{\mathcal{P}}_8 = \hat{P}_8\hat{P}_4\hat{P}_1 & T_8 \leq t < T_9, \\ \hat{\mathcal{P}}_9 = \hat{P}_4\hat{P}_1 & T_9 \leq t < T_{10}, \\ \hat{\mathcal{P}}_{10} = \hat{P}_1 & T_{10} \leq t < T_{11}, \\ \hat{\mathcal{P}}_{11} = \hat{P}_{11}\hat{P}_1 & T_{11} \leq t < T_{12}, \\ \hat{\mathcal{P}}_{12} = \hat{P}_1 & T_{12} \leq t < T_{13}, \\ \hat{\mathcal{P}}_{13} = \hat{1} & T_{13} \leq t < T. \end{cases} \quad (\text{B32})$$

$$\hat{P}_1 = e^{-i\hat{S}_{\text{tot}}^x \pi/2}, \quad (\text{B33})$$

$$\hat{P}_2 = e^{-i\hat{S}_{\text{tot}}^x \pi/2} \hat{V}_2 e^{i\hat{S}_{\text{tot}}^x \pi/2} = \exp \left\{ -i \sum_j [\hat{S}_{\mathbf{R}_j}^z (2\pi - (n_j + m_j)\pi/2)] \right\}, \quad (\text{B34})$$

$$\hat{P}_3 = e^{-i\hat{S}_{\text{tot}}^x \pi/2} \hat{V}_3 e^{i\hat{S}_{\text{tot}}^x \pi/2} = \hat{P}_2^\dagger, \quad (\text{B35})$$

$$\hat{P}_4 = e^{i\hat{S}_{\text{tot}}^y \pi/2}, \quad (\text{B36})$$

$$\hat{P}_5 = e^{i\hat{S}_{\text{tot}}^y \pi/2} e^{-i\hat{S}_{\text{tot}}^x \pi/2} \hat{V}_5 e^{i\hat{S}_{\text{tot}}^x \pi/2} e^{-i\hat{S}_{\text{tot}}^y \pi/2} = \hat{P}_2, \quad (\text{B37})$$

$$\hat{P}_6 = e^{i\hat{S}_{\text{tot}}^y \pi/2} e^{-i\hat{S}_{\text{tot}}^x \pi/2} \hat{V}_6 e^{i\hat{S}_{\text{tot}}^x \pi/2} e^{-i\hat{S}_{\text{tot}}^y \pi/2} = \hat{P}_3, \quad (\text{B38})$$

$$\hat{P}_7 = \hat{1}, \quad (\text{B39})$$

$$\hat{P}_8 = e^{i\hat{S}_{\text{tot}}^y \pi/2} e^{-i\hat{S}_{\text{tot}}^x \pi/2} \hat{V}_8 e^{i\hat{S}_{\text{tot}}^x \pi/2} e^{-i\hat{S}_{\text{tot}}^y \pi/2} = \exp \left\{ -i \sum_j [\hat{S}_{\mathbf{R}_j}^z (2\pi + (m_j - n_j)\pi/2)] \right\}, \quad (\text{B40})$$

$$\hat{P}_9 = e^{i\hat{S}_{\text{tot}}^y \pi/2} e^{-i\hat{S}_{\text{tot}}^x \pi/2} \hat{V}_9 e^{i\hat{S}_{\text{tot}}^x \pi/2} e^{-i\hat{S}_{\text{tot}}^y \pi/2} = \hat{P}_8^\dagger, \quad (\text{B41})$$

$$\hat{P}_{10} = \hat{P}_4^\dagger, \quad (\text{B42})$$

$$\hat{P}_{11} = e^{-i\hat{S}_{\text{tot}}^x \pi/2} \hat{V}_{11} e^{i\hat{S}_{\text{tot}}^x \pi/2} = \exp \left\{ -i \sum_j [\hat{S}_{\mathbf{R}_j}^z (2\pi + (n_j - m_j)\pi/2)] \right\}, \quad (\text{B43})$$

$$\hat{P}_{12} = e^{-i\hat{S}_{\text{tot}}^x \pi/2} \hat{V}_{12} e^{i\hat{S}_{\text{tot}}^x \pi/2} = \hat{P}_{11}^\dagger, \quad (\text{B44})$$

$$\hat{P}_{13} = \hat{P}_1^\dagger. \quad (\text{B45})$$

Appendix C: Derivation of the long-range interaction terms

In the main text, we assumed the nearest-neighbor interaction for simplicity in obtaining the effective Hamiltonian. However, the interaction between Rydberg atoms is, in fact, a long-range interaction because of the resonant dipole-dipole interaction. Therefore, in this Appendix, we consider long-range interactions beyond the nearest neighbor.

1. Next-nearest neighbor interaction

Here, we restrict our consideration to next-nearest neighbor interactions. The starting Hamiltonian is given by

$$\hat{H}_{XY}^{\text{NNN}} = \sum_{\sigma \in \{0,1\}} \sum_i J_{\mathbf{R}_i, \mathbf{R}_{i,\sigma}^{\text{NNN}}} (\hat{S}_{\mathbf{R}_i}^x \hat{S}_{\mathbf{R}_{i,\sigma}^{\text{NNN}}}^x + \hat{S}_{\mathbf{R}_i}^y \hat{S}_{\mathbf{R}_{i,\sigma}^{\text{NNN}}}^y), \quad (\text{C1})$$

where $\mathbf{R}_{i,\sigma}^{\text{NNN}} = a([n_i + 1]\mathbf{e}_x + [m_i + (-1)^\sigma]\mathbf{e}_y)$. Next, we apply the same pulses as mentioned in Sec. III of the main text. The Hamiltonian in the first rotating frame is written as

$$\hat{H}_1^{\text{NNN}}(t) \equiv \hat{U}_G^\dagger(t)[\hat{H}_{XY}^{\text{NNN}} + \hat{H}_L(t)]\hat{U}_G(t) \equiv \hat{H}_{XY1}^{\text{NNN}}(t) + \hat{H}_{L1}(t), \quad (\text{C2})$$

where

$$\hat{H}_{XY1}^{\text{NNN}}(t) = \begin{cases} \hat{H}_{XY}^{\text{NNN}}, & 0 \leq t < T_1, \\ \hat{H}_{ZX}^{\text{NNN}}, & T_1 \leq t < T_4, \\ \hat{H}_{YZ}^{\text{NNN}}, & T_4 \leq t < T_{10}, \\ \hat{H}_{ZX}^{\text{NNN}}, & T_{10} \leq t < T_{13}, \\ \hat{H}_{XY}^{\text{NNN}}, & T_{13} \leq t < T, \end{cases} \quad (\text{C3})$$

with

$$\hat{H}_{XY}^{\text{NNN}} = \sum_{\sigma \in \{0,1\}} \sum_i J_{\mathbf{R}_i, \mathbf{R}_{i,\sigma}^{\text{NNN}}} (\hat{S}_{\mathbf{R}_i}^x \hat{S}_{\mathbf{R}_{i,\sigma}^{\text{NNN}}}^x + \hat{S}_{\mathbf{R}_i}^y \hat{S}_{\mathbf{R}_{i,\sigma}^{\text{NNN}}}^y), \quad (\text{C4})$$

$$\hat{H}_{YZ}^{\text{NNN}} = \sum_{\sigma \in \{0,1\}} \sum_i J_{\mathbf{R}_i, \mathbf{R}_{i,\sigma}^{\text{NNN}}} (\hat{S}_{\mathbf{R}_i}^y \hat{S}_{\mathbf{R}_{i,\sigma}^{\text{NNN}}}^y + \hat{S}_{\mathbf{R}_i}^z \hat{S}_{\mathbf{R}_{i,\sigma}^{\text{NNN}}}^z), \quad (\text{C5})$$

$$\hat{H}_{ZX}^{\text{NNN}} = \sum_{\sigma \in \{0,1\}} \sum_i J_{\mathbf{R}_i, \mathbf{R}_{i,\sigma}^{\text{NNN}}} (\hat{S}_{\mathbf{R}_i}^z \hat{S}_{\mathbf{R}_{i,\sigma}^{\text{NNN}}}^z + \hat{S}_{\mathbf{R}_i}^x \hat{S}_{\mathbf{R}_{i,\sigma}^{\text{NNN}}}^x). \quad (\text{C6})$$

The Hamiltonian in the second rotating frame becomes

$$\hat{H}_2^{\text{NNN}}(t) \equiv \hat{U}_L^\dagger(t)\hat{H}_{XY1}^{\text{NNN}}(t)\hat{U}_L(t) \quad (\text{C7})$$

$$= \begin{cases} \hat{H}_{XY}^{\text{NNN}}, & 0 \leq t < T_1, \\ \hat{H}_{ZX}^{\text{NNN}}, & T_1 \leq t < T_2, \\ \sum_{\sigma \in \{0,1\}} \sum_i (-1)^{\sigma+1} J_{\mathbf{R}_i, \mathbf{R}_{i,\sigma}^{\text{NNN}}} (\hat{S}_{\mathbf{R}_i}^z \hat{S}_{\mathbf{R}_{i,\sigma}^{\text{NNN}}}^z + \hat{S}_{\mathbf{R}_i}^x \hat{S}_{\mathbf{R}_{i,\sigma}^{\text{NNN}}}^x), & T_2 \leq t < T_3, \\ \hat{H}_{ZX}^{\text{NNN}}, & T_3 \leq t < T_4, \\ \hat{H}_{YZ}^{\text{NNN}}, & T_4 \leq t < T_5, \\ \sum_{\sigma \in \{0,1\}} \sum_i (-1)^{\sigma+1} J_{\mathbf{R}_i, \mathbf{R}_{i,\sigma}^{\text{NNN}}} (\hat{S}_{\mathbf{R}_i}^y \hat{S}_{\mathbf{R}_{i,\sigma}^{\text{NNN}}}^y + \hat{S}_{\mathbf{R}_i}^z \hat{S}_{\mathbf{R}_{i,\sigma}^{\text{NNN}}}^z), & T_5 \leq t < T_6, \\ \hat{H}_{YZ}^{\text{NNN}}, & T_6 \leq t < T_7, \\ \hat{H}_{YZ}^{\text{NNN}}, & T_7 \leq t < T_8, \\ \sum_{\sigma \in \{0,1\}} \sum_i (-1)^\sigma J_{\mathbf{R}_i, \mathbf{R}_{i,\sigma}^{\text{NNN}}} (\hat{S}_{\mathbf{R}_i}^y \hat{S}_{\mathbf{R}_{i,\sigma}^{\text{NNN}}}^y + \hat{S}_{\mathbf{R}_i}^z \hat{S}_{\mathbf{R}_{i,\sigma}^{\text{NNN}}}^z), & T_8 \leq t < T_9, \\ \hat{H}_{YZ}^{\text{NNN}}, & T_9 \leq t < T_{10}, \\ \hat{H}_{ZX}^{\text{NNN}}, & T_{10} \leq t < T_{11}, \\ \sum_{\sigma \in \{0,1\}} \sum_i (-1)^\sigma J_{\mathbf{R}_i, \mathbf{R}_{i,\sigma}^{\text{NNN}}} (\hat{S}_{\mathbf{R}_i}^z \hat{S}_{\mathbf{R}_{i,\sigma}^{\text{NNN}}}^z + \hat{S}_{\mathbf{R}_i}^x \hat{S}_{\mathbf{R}_{i,\sigma}^{\text{NNN}}}^x), & T_{11} \leq t < T_{12}, \\ \hat{H}_{ZX}^{\text{NNN}}, & T_{12} \leq t < T_{13}, \\ \hat{H}_{XY}^{\text{NNN}}, & T_{13} \leq t < T_{14}. \end{cases} \quad (\text{C8})$$

Here, we set the propagation time as in Sec. III of the main text. The effective Hamiltonian restricted to next-nearest neighbor interactions is given by

$$\hat{H}_F^{(0),\text{NNN}} = \sum_{\sigma \in \{0,1\}} \sum_i J_F^{\text{NNN}} (\hat{\mathbf{S}}_{\mathbf{R}_i} \cdot \hat{\mathbf{S}}_{\mathbf{R}_{i,\sigma}^{\text{NNN}}}), \quad (\text{C9})$$

where $J_F^{\text{NNN}} \equiv 2\tau J_{\mathbf{R}_i, \mathbf{R}_{i,\sigma}^{\text{NNN}}}/T$. Therefore, when considering the next-nearest-neighbor interaction, we find that only the Heisenberg interaction appears. The reason why the DM interaction is absent is that the phase difference between site \mathbf{R}_i and site $\mathbf{R}_{i,\sigma}^{\text{NNN}}$ is always $\pm\pi$ [see Appendix A].

2. Next-next-nearest neighbor interaction

Here, we restrict our consideration to next-next-nearest neighbor interactions. The starting Hamiltonian is given by

$$\hat{H}_{XY}^{\text{NNNN}} = \sum_{\mu \in \{x,y\}} \sum_i J_{\mathbf{R}_i, \mathbf{R}_{i,\mu}^{\text{NNNN}}} (\hat{S}_{\mathbf{R}_i}^x \hat{S}_{\mathbf{R}_{i,\mu}^{\text{NNNN}}}^x + \hat{S}_{\mathbf{R}_i}^y \hat{S}_{\mathbf{R}_{i,\mu}^{\text{NNNN}}}^y), \quad (\text{C10})$$

where $\mathbf{R}_{i,\mu}^{\text{NNNN}} = \mathbf{R}_i + 2a\mathbf{e}_\mu$. Next, we apply the same pulses as mentioned in the main text. The Hamiltonian in the first rotating frame is written as

$$\hat{H}_1^{\text{NNNN}}(t) \equiv \hat{U}_G^\dagger(t) [\hat{H}_{XY}^{\text{NNNN}} + \hat{H}_L(t)] \hat{U}_G(t) \equiv \hat{H}_{XY1}^{\text{NNNN}}(t) + \hat{H}_{L1}(t), \quad (\text{C11})$$

where

$$\hat{H}_{XY1}^{\text{NNNN}}(t) = \begin{cases} \hat{H}_{XY}^{\text{NNNN}}, & 0 \leq t < T_1, \\ \hat{H}_{ZX}^{\text{NNNN}}, & T_1 \leq t < T_4, \\ \hat{H}_{YZ}^{\text{NNNN}}, & T_4 \leq t < T_{10}, \\ \hat{H}_{ZX}^{\text{NNNN}}, & T_{10} \leq t < T_{13}, \\ \hat{H}_{XY}^{\text{NNNN}}, & T_{13} \leq t < T, \end{cases} \quad (\text{C12})$$

with

$$\hat{H}_{XY}^{\text{NNNN}} \equiv \sum_{\mu \in \{x,y\}} \sum_i J_{\mathbf{R}_i, \mathbf{R}_{i,\mu}^{\text{NNNN}}} (\hat{S}_{\mathbf{R}_i}^x \hat{S}_{\mathbf{R}_{i,\mu}^{\text{NNNN}}}^x + \hat{S}_{\mathbf{R}_i}^y \hat{S}_{\mathbf{R}_{i,\mu}^{\text{NNNN}}}^y), \quad (\text{C13})$$

$$\hat{H}_{YZ}^{\text{NNNN}} \equiv \sum_{\mu \in \{x,y\}} \sum_i J_{\mathbf{R}_i, \mathbf{R}_{i,\mu}^{\text{NNNN}}} (\hat{S}_{\mathbf{R}_i}^y \hat{S}_{\mathbf{R}_{i,\mu}^{\text{NNNN}}}^y + \hat{S}_{\mathbf{R}_i}^z \hat{S}_{\mathbf{R}_{i,\mu}^{\text{NNNN}}}^z), \quad (\text{C14})$$

$$\hat{H}_{ZX}^{\text{NNNN}} \equiv \sum_{\mu \in \{x,y\}} \sum_i J_{\mathbf{R}_i, \mathbf{R}_{i,\mu}^{\text{NNNN}}} (\hat{S}_{\mathbf{R}_i}^z \hat{S}_{\mathbf{R}_{i,\mu}^{\text{NNNN}}}^z + \hat{S}_{\mathbf{R}_i}^x \hat{S}_{\mathbf{R}_{i,\mu}^{\text{NNNN}}}^x). \quad (\text{C15})$$

After then, we apply the same pulses again. The Hamiltonian in each propagation becomes

$$\hat{H}_2^{\text{NNNN}}(t) = \hat{U}_L^\dagger(t) \hat{H}_{XY1}^{\text{NNNN}}(t) \hat{U}_L(t) \quad (\text{C16})$$

$$= \begin{cases} \hat{H}_{XY}^{\text{NNNN}}, & 0 \leq t < T_1, \\ \hat{H}_{ZX}^{\text{NNNN}}, & T_1 \leq t < T_2, \\ -\hat{H}_{ZX}^{\text{NNNN}}, & T_2 \leq t < T_3, \\ \hat{H}_{ZX}^{\text{NNNN}}, & T_3 \leq t < T_4, \\ \hat{H}_{YZ}^{\text{NNNN}}, & T_4 \leq t < T_5, \\ -\hat{H}_{YZ}^{\text{NNNN}}, & T_5 \leq t < T_6, \\ \hat{H}_{YZ}^{\text{NNNN}}, & T_6 \leq t < T_7, \\ \hat{H}_{YZ}^{\text{NNNN}}, & T_7 \leq t < T_8, \\ -\hat{H}_{YZ}^{\text{NNNN}}, & T_8 \leq t < T_9, \\ \hat{H}_{YZ}^{\text{NNNN}}, & T_9 \leq t < T_{10}, \\ \hat{H}_{ZX}^{\text{NNNN}}, & T_{10} \leq t < T_{11}, \\ -\hat{H}_{ZX}^{\text{NNNN}}, & T_{11} \leq t < T_{12}, \\ \hat{H}_{ZX}^{\text{NNNN}}, & T_{12} \leq t < T_{13}, \\ \hat{H}_{XY}^{\text{NNNN}}, & T_{13} \leq t < T_{14}, \end{cases} \quad (\text{C17})$$

Here, we set the propagation time as in the main text. The effective Hamiltonian restricted to next-next-nearest neighbor interactions is given by

$$\hat{H}_F^{(0),\text{NNNN}} = \sum_{\mu \in \{x,y\}} \sum_i J_F^{\text{NNNN}} \left[(\tau - \tau_y) \hat{S}_{\mathbf{R}_i}^x \hat{S}_{\mathbf{R}_{i,\mu}^{\text{NNNN}}}^x + (\tau - \tau_x) \hat{S}_{\mathbf{R}_i}^y \hat{S}_{\mathbf{R}_{i,\mu}^{\text{NNNN}}}^y + (\tau - \tau_x - \tau_y) \hat{S}_{\mathbf{R}_i}^z \hat{S}_{\mathbf{R}_{i,\mu}^{\text{NNNN}}}^z \right], \quad (\text{C18})$$

where $J_F^{\text{NNNN}} \equiv 2\tau J_{\mathbf{R}_i, \mathbf{R}_{i,\mu}^{\text{NNNN}}}/T$. The reason why the DM interaction is absent is the same as in the case of the next-nearest-neighbor interaction.

Appendix D: Time evolution of spin expectation values

In this Appendix, we consider the Hamiltonian with Bloch-type DM interaction given by

$$\begin{aligned}\hat{H}_{\text{F,Bloch}}^{(0)} &= J_{\text{F}} \sum_{\langle i,j \rangle} \hat{\mathbf{S}}_{\mathbf{R}_i} \cdot \hat{\mathbf{S}}_{\mathbf{R}_j} + \sum_i \left[D_{x,\text{F}} (\hat{\mathbf{S}}_{\mathbf{R}_i} \times \hat{\mathbf{S}}_{\mathbf{R}_i+a\mathbf{e}_x})_x + D_{y,\text{F}} (\hat{\mathbf{S}}_{\mathbf{R}_i} \times \hat{\mathbf{S}}_{\mathbf{R}_i+a\mathbf{e}_y})_y \right] \\ &\equiv \hat{H}_{\text{ex}} + \hat{H}_{\text{DMx,x}} + \hat{H}_{\text{DMy,y}}.\end{aligned}\quad (\text{D1})$$

Now, we consider a symmetry of the Hamiltonian $\hat{H}_{\text{F,Bloch}}^{(0)}$. We define the space-inversion operator along the y direction \hat{I}_y and spin-inversion operators \hat{C}_μ as

$$\hat{I}_y^\dagger \hat{S}_{(R_j,x,R_j,y)}^\mu \hat{I}_y \equiv \hat{S}_{(R_j,x,L_y-R_j,y+a)}^\mu, \quad (\text{D2})$$

$$\hat{C}_\mu \equiv \prod_j (2\hat{S}_{\mathbf{R}_j}^\mu), \quad (\text{D3})$$

where $\mu = x, y, z$ and L_y represents the number of lattice sites along the y direction. For simplicity, we have assumed that L_y is even. From the above operations, we define the unitary operator

$$\hat{U}_s \equiv \hat{I}_y \hat{C}_x. \quad (\text{D4})$$

It is straightforward to show that the unitary operator \hat{U}_s commutes with $\hat{H}_{\text{F,Bloch}}^{(0)}$ and that $\hat{U}_s^\dagger \hat{S}_{\text{tot}}^{y,z} \hat{U}_s = -\hat{S}_{\text{tot}}^{y,z}$.

We now consider the equation of motion for the expectation values of $\hat{S}_{\text{tot}}^{y,z}$ with the initial condition $|\psi(t=0)\rangle \equiv \prod_{j=1}^N |+_j\rangle$:

$$i\hbar \frac{d}{dt} \langle \psi(t=0) | \hat{S}_{\text{tot}}^{y,z}(t) | \psi(t=0) \rangle = \langle \psi(t=0) | e^{i\hat{H}_{\text{F,Bloch}}^{(0)}t/\hbar} \left[\hat{S}_{\text{tot}}^{y,z}, \hat{H}_{\text{F,Bloch}}^{(0)} \right] e^{-i\hat{H}_{\text{F,Bloch}}^{(0)}t/\hbar} | \psi(t=0) \rangle. \quad (\text{D5})$$

Since the initial state $|\psi(t=0)\rangle$ is invariant to the space and spin inversion, one has the relation $\hat{U}_s |\psi(t=0)\rangle = |\psi(t=0)\rangle$. Using this relation and the symmetry properties of $\hat{H}_{\text{F,Bloch}}^{(0)}$ and $\hat{S}_{\text{tot}}^{y,z}$ with respect to \hat{U}_s described above, we obtain

$$\begin{aligned}i\hbar \frac{d}{dt} \langle \psi(t=0) | \hat{S}_{\text{tot}}^{y,z}(t) | \psi(t=0) \rangle &= \langle \psi(t=0) | e^{i\hat{H}_{\text{F,Bloch}}^{(0)}t/\hbar} \hat{U}_s^\dagger \left[\hat{S}_{\text{tot}}^{y,z}, \hat{H}_{\text{F,Bloch}}^{(0)} \right] \hat{U}_s e^{-i\hat{H}_{\text{F,Bloch}}^{(0)}t/\hbar} | \psi(t=0) \rangle \\ &= - \langle \psi(t=0) | e^{i\hat{H}_{\text{F,Bloch}}^{(0)}t/\hbar} \left[\hat{S}_{\text{tot}}^{y,z}, \hat{H}_{\text{F,Bloch}}^{(0)} \right] e^{-i\hat{H}_{\text{F,Bloch}}^{(0)}t/\hbar} | \psi(t=0) \rangle.\end{aligned}\quad (\text{D6})$$

Comparing Eq. (D6) with (D5), we conclude that

$$i\hbar \frac{d}{dt} \langle \psi(t=0) | \hat{S}_{\text{tot}}^{y,z}(t) | \psi(t=0) \rangle = 0. \quad (\text{D7})$$

Since the expectation values of $\hat{S}_{\text{tot}}^{y,z}$ are zero at the initial time $t=0$, they are always zero.

-
- | | |
|---|--|
| <p>[1] S. Lloyd, <i>Science</i> 273, 1073 (1996).
 [2] R. P. Feynman, <i>Int. J. Theor. Phys.</i> 21, 467 (1982).
 [3] D. S. Abrams and S. Lloyd, <i>Phys. Rev. Lett.</i> 83, 5162 (1999).
 [4] F. Schäfer, T. Fukuhara, S. Sugawa, Y. Takasu, and Y. Takahashi, <i>Nat. Rev. Phys.</i> 2, 411 (2020).
 [5] C. Monroe, W. C. Campbell, L.-M. Duan, Z.-X. Gong, A. V. Gorshkov, P. W. Hess, R. Islam, K. Kim, N. M. Linke, G. Pagano, P. Richerme, C. Senko, and N. Y. Yao, <i>Rev. Mod. Phys.</i> 93, 025001 (2021).</p> | <p>[6] R. Blatt and C. F. Roos, <i>Nat. Phys.</i> 8, 277 (2012).
 [7] B. Yan, S. A. Moses, B. Gadway, J. P. Covey, K. R. Hazzard, A. M. Rey, D. S. Jin, and J. Ye, <i>Nature</i> 501, 521 (2013).
 [8] Y. L. Zhou, M. Ortner, and P. Rabl, <i>Phys. Rev. A</i> 84, 052332 (2011).
 [9] E. Altman, K. R. Brown, G. Carleo, L. D. Carr, E. Demler, C. Chin, B. DeMarco, S. E. Economou, M. A. Eriksson, K.-M. C. Fu, M. Greiner, K. R. Hazzard, R. G. Hulet, A. J. Kollár, B. L. Lev, M. D. Lukin, R. Ma,</p> |
|---|--|

- X. Mi, S. Misra, C. Monroe, K. Murch, Z. Nazario, K.-K. Ni, A. C. Potter, P. Roushan, M. Saffman, M. Schleier-Smith, I. Siddiqi, R. Simmonds, M. Singh, I. Spielman, K. Temme, D. S. Weiss, J. Vučković, V. Vuletić, J. Ye, and M. Zwerlein, *PRX quantum* **2**, 017003 (2021).
- [10] M. Kjaergaard, M. E. Schwartz, J. Braumüller, P. Krantz, J. I.-J. Wang, S. Gustavsson, and W. D. Oliver, *Annu. Rev. Condens. Matter Phys.* **11**, 369 (2020).
- [11] G. Wendin, *Rep. Prog. Phys.* **80**, 106001 (2017).
- [12] A. Browaeys and T. Lahaye, *Nat. Phys.* **16**, 132 (2020).
- [13] H. Weimer, M. Müller, I. Lesanovsky, P. Zoller, and H. P. Büchler, *Nat. Phys.* **6**, 382 (2010).
- [14] J. Zhang, G. Pagano, P. W. Hess, A. Kyprianidis, P. Becker, H. Kaplan, A. V. Gorshkov, Z.-X. Gong, and C. Monroe, *Nature* **551**, 601 (2017).
- [15] C. Chen, G. Bornet, M. Bintz, G. Emperauger, L. Leclerc, V. S. Liu, P. Scholl, D. Barredo, J. Hauschild, S. Chatterjee, M. Schuler, A. M. Läuchli, M. P. Zaletel, T. Lahaye, N. Y. Yao, and A. Browaeys, *Nature* **616**, 691 (2023).
- [16] P. Scholl, M. Schuler, H. J. Williams, A. A. Eberharter, D. Barredo, K.-N. Schymik, V. Lienhard, L.-P. Henry, T. C. Lang, T. Lahaye, A. M. Läuchli, and A. Browaeys, *Nature* **595**, 233 (2021).
- [17] S. Ebadi, T. T. Wang, H. Levine, A. Keesling, G. Semeghini, A. Omran, D. Bluvstein, R. Samajdar, H. Pichler, W. W. Ho, S. Choi, S. Sachdev, M. Greiner, V. Vuletić, and M. D. Lukin, *Nature* **595**, 227 (2021).
- [18] H. Bernien, S. Schwartz, A. Keesling, H. Levine, A. Omran, H. Pichler, S. Choi, A. S. Zibrov, M. Endres, M. Greiner, V. Vuletić, and M. D. Lukin, *Nature* **551**, 579 (2017).
- [19] H. Kim, Y. Park, K. Kim, H.-S. Sim, and J. Ahn, *Phys. Rev. Lett.* **120**, 180502 (2018).
- [20] C. Gross and I. Bloch, *Science* **357**, 995 (2017).
- [21] H. Labuhn, D. Barredo, S. Ravets, S. De Léséleuc, T. Macrì, T. Lahaye, and A. Browaeys, *Nature* **534**, 667 (2016).
- [22] J. Zeiher, J.-y. Choi, A. Rubio-Abadal, T. Pohl, R. Van Bijnen, I. Bloch, and C. Gross, *Phys. Rev. X* **7**, 041063 (2017).
- [23] S. De Léséleuc, S. Weber, V. Lienhard, D. Barredo, H. P. Büchler, T. Lahaye, and A. Browaeys, *Phys. Rev. Lett.* **120**, 113602 (2018).
- [24] V. Lienhard, S. de Léséleuc, D. Barredo, T. Lahaye, A. Browaeys, M. Schuler, L.-P. Henry, and A. M. Läuchli, *Phys. Rev. X* **8**, 021070 (2018).
- [25] E. Guardado-Sanchez, P. T. Brown, D. Mitra, T. Devakul, D. A. Huse, P. Schauß, and W. S. Bakr, *Phys. Rev. X* **8**, 021069 (2018).
- [26] A. Keesling, A. Omran, H. Levine, H. Bernien, H. Pichler, S. Choi, R. Samajdar, S. Schwartz, P. Silvi, S. Sachdev, P. Zoller, M. Endres, M. Greiner, V. Vuletić, and M. D. Lukin, *Nature* **568**, 207 (2019).
- [27] G. Semeghini, H. Levine, A. Keesling, S. Ebadi, T. T. Wang, D. Bluvstein, R. Verresen, H. Pichler, M. Kalinowski, R. Samajdar, A. Omran, S. Sachdev, A. Vishwanath, M. Greiner, V. Vuletić, and M. D. Lukin, *Science* **374**, 1242 (2021).
- [28] D. Bluvstein, A. Omran, H. Levine, A. Keesling, G. Semeghini, S. Ebadi, T. T. Wang, A. A. Michailidis, N. Maskara, W. W. Ho, S. Choi, M. Serbyn, M. Greiner, V. Vuletić, and M. D. Lukin, *Science* **371**, 1355 (2021).
- [29] V. Bharti, S. Sugawa, M. Mizoguchi, M. Kunimi, Y. Zhang, S. de Léséleuc, T. Tomita, T. Franz, M. Weidemüller, and K. Ohmori, *Phys. Rev. Lett.* **131**, 123201 (2023).
- [30] A. P. Orioli, A. Signoles, H. Wildhagen, G. Günter, J. Berges, S. Whitlock, and M. Weidemüller, *Phys. Rev. Lett.* **120**, 063601 (2018).
- [31] S. De Léséleuc, V. Lienhard, P. Scholl, D. Barredo, S. Weber, N. Lang, H. P. Büchler, T. Lahaye, and A. Browaeys, *Science* **365**, 775 (2019).
- [32] A. Signoles, T. Franz, R. F. Alves, M. Gärttner, S. Whitlock, G. Zürn, and M. Weidemüller, *Phys. Rev. X* **11**, 011011 (2021).
- [33] P. Scholl, H. J. Williams, G. Bornet, F. Wallner, D. Barredo, L. Henriët, A. Signoles, C. Hainaut, T. Franz, S. Geier, A. Tebben, A. Salzinger, G. Zürn, T. Lahaye, M. Weidemüller, and A. Browaeys, *PRX Quantum* **3**, 020303 (2022).
- [34] T. Franz, S. Geier, C. Hainaut, A. Signoles, N. Thaicharoen, A. Tebben, A. Salzinger, A. Braemer, M. Gärttner, G. Zürn, G. Zürn, and M. Weidemüller, *arXiv preprint arXiv:2207.14216* (2022).
- [35] T. Franz, S. Geier, C. Hainaut, A. Braemer, N. Thaicharoen, M. Hornung, E. Braun, M. Gärttner, G. Zürn, and M. Weidemüller, *Phys. Rev. Res.* **6**, 033131 (2024).
- [36] S. Geier, N. Thaicharoen, C. Hainaut, T. Franz, A. Salzinger, A. Tebben, D. Grimshandl, G. Zürn, and M. Weidemüller, *Science* **374**, 1149 (2021).
- [37] L.-M. Steinert, P. Osterholz, R. Eberhard, L. Festa, N. Lorenz, Z. Chen, A. Trautmann, and C. Gross, *Phys. Rev. Lett.* **130**, 243001 (2023).
- [38] N. Nishad, A. Keselman, T. Lahaye, A. Browaeys, and S. Tsesses, *Phys. Rev. A* **108**, 053318 (2023).
- [39] M. Kunimi, T. Tomita, H. Katsura, and Y. Kato, *Phys. Rev. A* **110**, 043312 (2024).
- [40] F. Percivalle, D. Rossini, T. Haug, O. Morsch, and L. Amico, *Phys. Rev. A* **108**, 023305 (2023).
- [41] E. Kuznetsova, S. Mistakidis, S. T. Rittenhouse, S. F. Yelin, and H. Sadeghpour, *arXiv preprint arXiv:2309.08795* (2023).
- [42] M. Kalinowski, N. Maskara, and M. D. Lukin, *Phys. Rev. X* **13**, 031008 (2023).
- [43] Y.-H. Chen, B.-Z. Wang, T.-F. J. Poon, X.-C. Zhou, Z.-X. Liu, and X.-J. Liu, *arXiv preprint arXiv:2310.12905* (2023).
- [44] I. Dzyaloshinsky, *J. Phys. Chem. Solids* **4**, 241 (1958).
- [45] T. Moriya, *Phys. Rev.* **120**, 91 (1960).
- [46] Y. Togawa, T. Koyama, K. Takayanagi, S. Mori, Y. Kousaka, J. Akimitsu, S. Nishihara, K. Inoue, A. Ovchinnikov, and J.-i. Kishine, *Phys. Rev. Lett.* **108**, 107202 (2012).
- [47] J.-i. Kishine, K. Inoue, and Y. Yoshida, *Prog. Theor. Phys. Suppl.* **159**, 82 (2005).
- [48] T. Skyrme, *Nucl. Phys.* **31**, 556 (1962).
- [49] A. N. Bogdanov and D. Yablonskii, *Zh. Eksp. Teor. Fiz* **95**, 178 (1989).
- [50] S. Mühlbauer, B. Binz, F. Jonietz, C. Pfleiderer, A. Rosch, A. Neubauer, R. Georgii, and P. Böni, *Science* **323**, 915 (2009).
- [51] Y. Tokura and N. Kanazawa, *Chem. Rev.* **121**, 2857 (2020).
- [52] A. Haller, S. Groenendijk, A. Habibi, A. Michels, and T. L. Schmidt, *Phys. Rev. Res.* **4**, 043113 (2022).

- [53] N. Goldman and J. Dalibard, *Phys. Rev. X* **4**, 031027 (2014).
- [54] M. Bukov, L. D'Alessio, and A. Polkovnikov, *Adv. Phys.* **64**, 139 (2015).
- [55] S. de Léséleuc, D. Barredo, V. Lienhard, A. Browaeys, and T. Lahaye, *Phys. Rev. Lett.* **119**, 053202 (2017).
- [56] G. Bornet, G. Emperauger, C. Chen, F. Machado, S. Chern, L. Leclerc, B. Gély, Y. T. Chew, D. Barredo, T. Lahaye, N. Y. Yao, and A. Browaeys, *Phys. Rev. Lett.* **132**, 263601 (2024).
- [57] T. G. Walker and M. Saffman, *J. Phys. B: At. Mol. Opt. Phys.* **38**, S309 (2005).
- [58] D. Barredo, H. Labuhn, S. Ravets, T. Lahaye, A. Browaeys, and C. S. Adams, *Phys. Rev. Lett.* **114**, 113002 (2015).
- [59] S. Ravets, H. Labuhn, D. Barredo, L. Béguin, T. Lahaye, and A. Browaeys, *Nat. Phys.* **10**, 914 (2014).
- [60] C. Chen, G. Emperauger, G. Bornet, F. Caleca, B. Gély, M. Bintz, S. Chatterjee, V. Liu, D. Barredo, N. Y. Yao, L. Thierry, M. Fabio, R. Tommaso, and B. Antoine, arXiv preprint arXiv:2311.11726 (2023).
- [61] T. Kuwahara, T. Mori, and K. Saito, *Ann. Phys.* **367**, 96 (2016).
- [62] A. Derras-Chouk, E. M. Chudnovsky, and D. A. Garanin, *Phys. Rev. B* **98**, 024423 (2018).
- [63] F. Mahfouzi and N. Kioussis, *Phys. Rev. B* **103**, 094410 (2021).
- [64] C. Sheng, J. Hou, X. He, K. Wang, R. Guo, J. Zhuang, B. Mamat, P. Xu, M. Liu, J. Wang, and M. Zhan, *Phys. Rev. Lett.* **128**, 083202 (2022).
- [65] K. Singh, S. Anand, A. Pocklington, J. T. Kemp, and H. Bernien, *Phys. Rev. X* **12**, 011040 (2022).
- [66] K. Singh, C. E. Bradley, S. Anand, V. Ramesh, R. White, and H. Bernien, *Science* **380**, 1265 (2023).
- [67] S. Blanes, F. Casas, J.-A. Oteo, and J. Ros, *Phys. Rep.* **470**, 151 (2009).
- [68] J. Haegeman, *Krylovkit* (2024).